Capacity Analysis Under Generalized Composite Fading Conditions

(Invited Paper)

Paschalis C. Sofotasios*,‡, Seong Ki Yoo§, Nidhi Bhargav§, Sami Muhaidat*, Simon L. Cotton§, Michail Matthaiou§, Mikko Valkama‡, and George K. Karagiannidis¶

*Department of Electrical and Computer Engineering, Khalifa University of Science and Technology, P. O. Box 127788, Abu Dhabi, United Arab Emirates (e-mail: paschalis.sofotasios; sami.muhaidat@ku.ac.ae)
‡Department of Electronics and Communications Engineering, Tampere University of Technology, FI-33101, Tampere, Finland (e-mail: {paschalis.sofotasios; mikko.e.valkama}@tut.fi)
§Institute of Electronics, Communications and Information Technology, Queen's University Belfast, BT3 9DT, Belfast, United Kingdom (e-mail: {syoo02; nbhargav01; simon.cotton; m.matthaiou}@qub.ac.uk)
¶Department of Electrical and Computer Engineering, Aristotle University of Thessaloniki, GR-51124, Thessaloniki, Greece (e-mail: geokarag@auth.gr)

***Abstract*—Novel composite fading models were recently proposed based on inverse gamma distributed shadowing conditions. These models were extensively shown to provide remarkable modeling of the simultaneous occurrence of multipath fading and shadowing phenomena in emerging wireless scenarios such as cellular, off-body and vehicle-to-vehicle communications. Furthermore, the algebraic representation of these models is rather tractable, which renders them convenient to handle both analytically and numerically. The present contribution presents the major theoretical and practical characteristics of the $\eta-\mu$ / inverse gamma composite fading model, followed by a thorough ergodic capacity analysis. To this end, novel analytic expressions are derived, which are subsequently used in the evaluation of the corresponding system performance. In this context, the offered results are compared with respective results from cases assuming conventional fading conditions, which leads to the development of numerous insights on the effect of the multipath fading and shadowing severity on the achieved capacity levels. It is expected that these results will be useful in the design of timely and highly demanding wireless technologies, such as wearable, cellular and inter-vehicular communications as well in wireless power transfer based applications in the context of the Internet of Things.**

I. Introduction

Accurate characterization and modeling of fading channels constitutes a core topic in wireless communications as fading phenomena affect considerably the performance of conventional and emerging communication systems. As a result, numerous fading models which provide adequate modeling accuracy to specific types of fading conditions have been proposed during the past years [1]–[4] and the references therein. In this context, it has been extensively shown that generalized fading models are capable of providing accurate characterization of multipath fading [5]–[10]. Yet, it has been also shown that multipath fading and shadowing phenomena practically occur simultaneously and can be modeled with the aid of composite fading distributions [5], [11]–[23]. However, many of the existing composite fading models proposed in the open technical literature do not typically provide holistic accurate modeling of fading phenomena. Moreover, they often have a complicated mathematical form, which renders them analytically intractable in numerous applications of interest. Motivated by this, the authors in [1]–[3] proposed two novel distributions, namely the $\kappa-\mu$ / inverse gamma and the $\eta-\mu$ / inverse gamma that constitute effective composite fading models. Their high modeling capability has been validated by their exemplary fit to results obtained from extensive measurement campaigns. These campaigns included communication scenarios in the context of wearable, cellular and vehicular communications, which constitute emerging and timely topics of interest. In addition, a distinct characteristic of the proposed models is their relatively convenient algebraic representation, which renders them tractable both analytically and numerically. Based on this, they overall constitute the most adequate balance between modeling accuracy and algebraic tractability compared to the existing composite fading models in the open technical literature.

It is recalled that fading distributions have been extensively used in the analysis and evaluation of wireless communications since they typically allow the derivation of explicit expressions for critical performance measures of interest. However, this task becomes considerably more challenging, if not impossible, in the case of generalized and/or composite fading conditions [6], [24]. Based on this, the authors in [26]–[28] analyzed the capacity over generalized fading channels under different adaptation policies. This topic was also addressed in [29] for the case of K_{G} fading channels, in [13] and [30] for the case of $\mathcal{G}$ fading channels and in [31] and [32] for the case of $\eta-\mu$ / gamma and $\kappa-\mu$ shadowed fading channels, respectively. In

978-1-5386-4609-0/18/$31.00 ©2018 IEEE

the same context, the outage probability (OP) over different generalized interference-limited scenarios was investigated in [33], whereas an analytical framework for the case of device-to-device communications in cellular networks was proposed in [34]. Finally, the outage capacity (OC) of orthogonal space-time block codes over multi-cluster scattering multi-antenna systems as well as the coverage capacity 5G millimeter wave cellular systems were addressed in [35] and [36], respectively.

Motivated by the above, the present work analyzes the channel capacity of digital communications over $\eta-\mu$ / inverse gamma composite fading channels. To this end, we derive an explicit analytic expression for the ergodic capacity under these composite fading conditions in the form of a simple and convergent infinite series. An elegant upper bound for the corresponding truncation error is also derived in closed-form, allowing the precise determination of the number of terms required for given accuracy levels. Particularly in the considered case of the ergodic capacity, it is shown that few terms are required to achieve a 1% accuracy, which is practically sufficient for channel capacity relating measures. Based on this, the derived expressions are utilized in quantifying the effects of different fading conditions on the corresponding system performance. This leads to the development of insights which are expected to be useful in the design of emerging wireless technologies such as cellular, wearable and vehicular communications, including applications relating to wireless powering of devices in the context of the Internet of Things.

The remainder of this paper is organized as follows: Section II revisits the basic characteristics and properties of the recently proposed $\eta-\mu$ / inverse gamma fading model. Capitalizing on this, Section III is devoted to the analysis of the ergodic capacity under these fading conditions, followed by the corresponding numerical results and related discussions in Section IV. Finally, closing remarks are given in Section V.

II. The η-μ / Inverse Gamma Fading Model

A. Statistics and Physical Interpretation

Similar to the physical signal model proposed for the η-μ fading channel [2], the received signal in an η-μ / inverse gamma composite fading channel is composed of separable clusters of multipath waves propagating in a non-homogeneous environment. In *Format* 1, the in-phase and quadrature components of the fading signal within each cluster are assumed to be statistically independent and to have different power. On the other hand, in *Format* 2, the in-phase and quadrature components of the fading signal within each cluster are assumed to be correlated and to have identical power. Unlike in the η-μ fading model, in the η-μ / inverse gamma model the mean power of the scattered waves is randomly fluctuated due to shadowing. Following this definition, the composite signal envelope, R, in an η-μ / inverse gamma composite fading channel can be expressed as

$$R=\sqrt{\sum_{i=1}^{n_s} AI_i^2+AQ_i^2} \tag{1}$$

where n_s denotes the number of clusters of multipath and A represents an inverse gamma RV. In *Format* 1, I_i and Q_i are mutually independent Gaussian RVs with $\mathbb{E}[I_i]=\mathbb{E}[Q_i]=0$, $\mathbb{E}\left[I_i^2\right]=\sigma_I^2$ and $\mathbb{E}\left[Q_i^2\right]=\sigma_Q^2$; in *Format* 2, I_i and Q_i are mutually correlated Gaussian RVs with $\mathbb{E}[I_i]=\mathbb{E}[Q_i]=0$, and $\mathbb{E}\left[I_i^2\right]=\mathbb{E}\left[Q_i^2\right]=\sigma^2$. To this effect, the envelope probability density function (PDF) of the η-μ / inverse gamma composite fading model is expressed as [2], [3]

$$f_R(r)=\frac{2^{2\mu+1}\mu^{2\mu}\,h^{\mu}(m_s\Omega)^{m_s}r^{4\mu-1}}{B\left(m_s,2\mu\right)\left(2\mu hr^2+m_s\Omega\right)^{m_s+2\mu}} \times{}_2F_1\left(\frac{m_s+2\mu}{2},\frac{m_s+2\mu+1}{2};\frac{2\mu+1}{2};\frac{\left(2\mu Hr^2\right)^2}{\left(2\mu hr^2+m_s\Omega\right)^2}\right) \tag{2}$$

where $\Gamma(\cdot)$ and $B(\cdot,\cdot)$ the gamma [38, Eq. (8.310.1)] and Beta functions [38, Eq. (8.384.1)], respectively, whereas ${}_2F_1(\cdot,\cdot;\cdot;\cdot)$ is the Gauss hypergeometric function [38, Eq. (9.111)]. In terms of its physical interpretation, μ is related to the number of multipath clusters while m_s is the scale parameter of the distribution which accounts for shadowing. Also, η is defined as $\eta=\sigma_I^2/\sigma_Q^2$ (i.e. the scattered wave power ratio between the in-phase and quadrature components of each cluster of multipath) in *Format* 1, whereas $\eta=\mathbb{E}[I_iQ_i]/\sigma^2$ (i.e. the correlation coefficient between the in-phase and quadrature components) in *Format* 2. Accordingly, $h=(2+\eta^{-1}+\eta)/4$ and $H=(\eta^{-1}-\eta)/4$ in $Format\,1$, while $h=1/(1-\eta^2)$ and $H=\eta/(1-\eta^2)$ in $Format\,2$. Thus, $Format\,1$ can be obtained from $Format\,2$ and vice versa by using the following relationship $\eta_{Format1}=(1-\eta_{Format2})/(1+\eta_{Format2})$ or, equivalently by $\eta_{Format2}=(1-\eta_{Format1})/(1+\eta_{Format1})$, where $0<\eta_{Format1}<\infty$ in $Format\,1$ and $-1<\eta_{Format2}<1$ in $Format\,2$. In this model, the mean signal power is given by $\mathbb{E}\left[R^2\right]=\Omega=\mu\left(1+\eta^{-1}\right)\sigma_I^2=\mu\left(1+\eta\right)\sigma_Q^2$ in *Format* 1 and by $\mathbb{E}\left[R^2\right]=\Omega=2\mu\sigma^2$ in *Format* 2.

Based on the above, the PDF of the instantaneous SNR of the η-μ / inverse gamma composite model is expressed as [3]

$$f_\gamma(\gamma)=\frac{2^{2\mu}\mu^{2\mu}\,h^{\mu}(m_s\overline{\gamma})^{m_s}\gamma^{2\mu-1}}{B(m_s,2\mu)(2\mu h\gamma+m_s\overline{\gamma})^{m_s+2\mu}} \times{}_2F_1\left(\frac{m_s+2\mu}{2},\frac{m_s+2\mu+1}{2};\frac{2\mu+1}{2};\frac{(2\mu H\gamma)^2}{(2\mu h\gamma+m_s\overline{\gamma})^2}\right) \tag{3}$$

whereas the corresponding CDF is given by [3]

$$F_\gamma(\gamma)=\frac{2^{2\mu-1}h^{\mu}}{\Gamma(m_s)\Gamma(2\mu)}\sum_{i=0}^{\infty}\frac{\Gamma\left(m_s+2\mu+2i\right)H^{2i}}{i!\left(\frac{2\mu+1}{2}\right)_i\left(\mu+i\right)}\left(\frac{\mu\gamma}{m_s\overline{\gamma}}\right)^{2\mu+2i} \times{}_2F_1\left(m_s+2\mu+2i,2\mu+2i;2\mu+2i+1;-\frac{2\mu h\gamma}{m_s\overline{\gamma}}\right) \tag{4}$$

where $(\cdot)_i$ denotes the Pochhammer symbol [38]–[41]. The tractable closed-form upper bound in (5), at the top of the next page, was derived for the truncation error of the infinite series

$$\mathcal{T} \leq \frac{\Gamma(m_s+2\mu)\,(\mu\gamma)^{2\mu}}{(\mu+T_0)(m_s\bar{\gamma})^{2\mu}}\;{}_2F_1\!\left(m_s+2\mu+2T_0,2\mu+2T_0;2\mu+2T_0+1;-\frac{2\mu h\gamma}{m_s\bar{\gamma}}\right)\;{}_2F_1\!\left(\frac{m_s+2\mu}{2},\frac{m_s+2\mu+1}{2};\frac{2\mu+1}{2};\left(\frac{2\mu\gamma H}{m_s\bar{\gamma}}\right)^2\right) \tag{5}$$

in (4), whereas the corresponding n^{th} moments are given by

$$\mathbb{E}\left[\gamma^n\right] = \frac{B\left(m_s-n,2\mu+n\right)}{B\left(m_s,2\mu\right)h^{\mu}}\left(\frac{m_s\bar{\gamma}}{2\mu h}\right)^n \times {}_2F_1\left(\mu+\frac{n}{2},\mu+\frac{n}{2}+\frac{1}{2};\mu+\frac{1}{2};\frac{H^2}{h^2}\right). \tag{6}$$

Likewise, the moment-generating function (MGF) of the η-μ / inverse gamma composite model was derived in [3], namely

$$M_\gamma(-s)=\sum_{i=0}^{\infty}\frac{\Gamma\left(\mu+i\right)H^{2i}}{i!\,\Gamma(\mu)\,h^{\mu+2i}}\left[{}_1F_1\left(2\mu+2i;1-m_s;\frac{sm_s\bar{\gamma}}{2\mu h}\right) +\left(\frac{sm_s\bar{\gamma}}{2\mu h}\right)^{m_s}\frac{\Gamma(-m_s)}{B(m_s,2\mu+2i)}\,{}_1F_1\left(m_s+2\mu+2i;1+m_s;\frac{sm_s\bar{\gamma}}{2\mu h}\right)\right] \tag{7}$$

along with the following elegant closed-form upper bound for the involved truncation error

$$\mathcal{T} \leq {}_1F_1\left(2\mu+2T_0;1-m_s;\frac{sm_s\bar{\gamma}}{2\mu h}\right){}_1F_0\left(\mu;-;\frac{H^2}{h^2}\right) - \left[{}_1F_1\left(m_s+2\mu+2T_0;1+m_s;\frac{sm_s\bar{\gamma}}{2\mu h}\right) \times {}_2F_1\left(\frac{m_s+2\mu}{2},\frac{m_s+2\mu+1}{2};\frac{2\mu+1}{2};\frac{H^2}{h^2}\right)\right]. \tag{8}$$

B. Numerical and Measurement Results

A key advantage of the η-μ / inverse gamma model is that it inherits all of the generality of the η-μ model. Also, the m_s parameter controls the amount of the shadowing of the mean signal power. Thus, as $m_s \to 0$, the scattered signal component are completely shadowed. On the contrary, as $m_s \to \infty$, there is no shadowing present in the channel and thus the mean signal power becomes deterministic and the η-μ / inverse gamma model coincides with the η-μ model. Therefore, by setting μ = 1/2, and $m_s \to \infty$, the Nakagami-q (or Hoyt) fading model is deduced where η becomes equivalent to the square of the q parameter of Nakagami-q fading model (i.e. $\eta = q^2$). The Nakagami-m fading model can be obtained by letting $m_s \to \infty$ and $\eta \to 0$ with the μ parameter becoming equivalent to the m parameter of Nakagami-m fading model. Based on this, the Rayleigh fading model can also be readily obtained by setting $\mu = m = 1$.

It is worth highlighting that the η-μ / inverse gamma model can be also used to provide an accurate approximation of other lognormal- and gamma-based composite fading models. For example, it can provide a good match to the Rayleigh / lognormal (u, σ) [37], Rayleigh / gamma (a, b) [11] and Nakagami-m / gamma (m, a, b) [25] composite fading models. For this comparison, the m_s and Ω parameters of the η-μ / inverse gamma composite fading model were estimated from the u and σ parameters of the Rayleigh / lognormal model and from the a and b parameters of the Rayleigh / gamma and Nakagami-m / gamma models by matching their first and second moments, such that

$$m_s = \frac{2\exp(\sigma^2)-1}{\exp(\sigma^2)-1}, \qquad \Omega = \frac{\exp(u+\frac{3}{2}\sigma^2)}{m_s(\exp(\sigma^2)-1)} \tag{9}$$

and

$$m_s = a+2, \qquad \Omega = \frac{ab(a+1)}{m_s}. \tag{10}$$

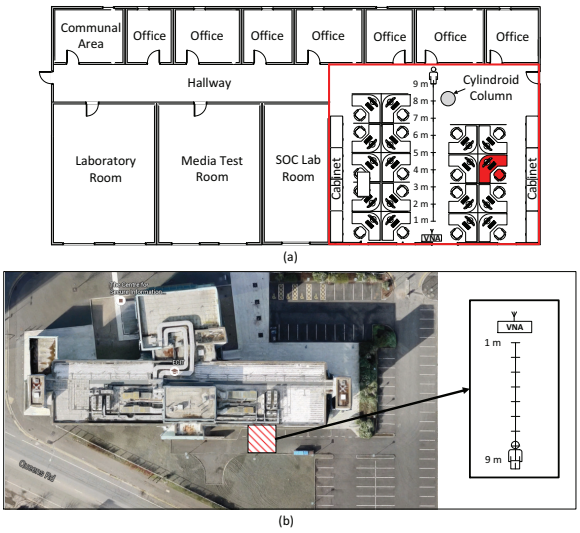

Fig. 1: (a) Indoor open office (99.63 m^2) and (b) outdoor car parking environments used for the wearable off-body measurements. The desk filled with red color in (a) denotes that one person was working at his desk during the measurement in an open office area environment.

C. Application in Wearable Communication Channels

The applicability of the η-μ / inverse gamma composite fading model was demonstrated in three realistic practical communication scenarios [3]. First, this was realized in the context of the emerging area of wearable communications which have recently received significant attention due to the wide range of promising application areas including medical, sports, military and entertainment [3] and the references therein. The first set of wearable off-body channel measurements were conducted in an indoor open office area environment [red rectangle: 10.62 m $\times$ 12.23 m, Fig. 1(a)] situated on the 1$^{\text{st}}$ floor of the Institute of Electronics, Communications and Information Technology (ECIT) at Queen's University Belfast in the United Kingdom. The ECIT building consists of metal studded dry wall with a metal tiled floor covered with polypropylene fiber,

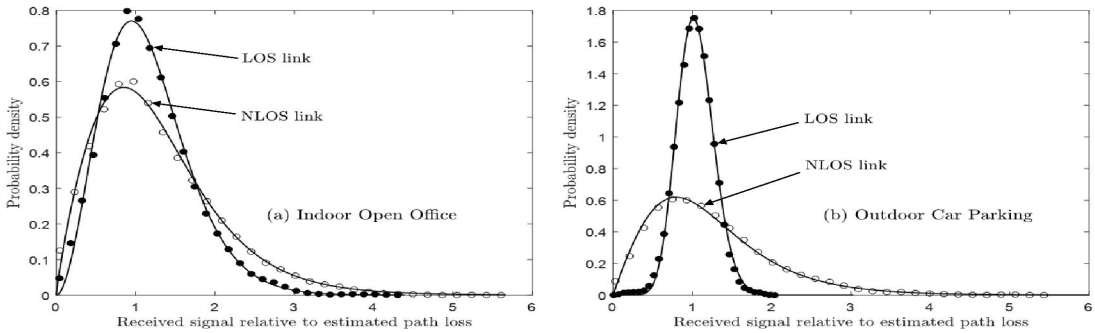

Fig. 2: Empirical PDFs (symbols) of the composite fading signal observed in the LOS and NLOS wearable off-body links for the (a) indoor open office and (b) outdoor car parking environments compared to the theoretical probability for the η-μ / inverse gamma (dotted lines) composite fading model.

rubber backed carpet tiles, and metal ceiling with mineral fiber tiles and recessed louvered luminaries suspended 2.70 m above floor level. As shown in Fig. 1(a), the open office area contained a number of soft partitions, cabinets, PCs, chairs and desks. During the channel measurements, one person was working at his desk. To improve the generality of the field validations conducted here, another set of measurements was performed in a more sparse environment, namely an outdoor car parking area adjacent to the ECIT building, as shown in Fig. 1(b) [3]. The transmitter (TX) used for the measurements consisted of an ML5805 transceiver manufactured by RFMD, which was configured to transmit a continuous wave signal with an output power of $+17.6$ dBm at 5.8 GHz. During the wearable off-body measurements, the TX antenna was positioned on the front-central waist region of an adult male of height 1.83 m and mass 73 kg using a small strip of Velcro®. For the receiver (RX), a single antenna was positioned on a non-conductive polyvinyl chloride (PVC) pole at height of 1.10 m above the floor level so that it was vertically polarized. It was then connected to port 1 of a Rohde & Schwarz ZVB-8 Vector Network Analyzer (VNA) using a low-loss coaxial cable. A pre-measurement calibration was conducted to reduce the effects of known system based errors using a Rohde & Schwarz ZV-Z51 calibration unit. This also enabled the elimination of the effects of the power amplifier and cable loss. The VNA was configured as a sampling RX, recording the magnitude of the b_1 wave quantity incident on port 1 with a bandwidth of 10 kHz (centered at the operation frequency of 5.8 GHz). The b_1 measurements were automatically collected and stored on a laptop through a local area network (LAN) connection, providing an effective channel sampling frequency of 425.6 Hz. Both the TX and RX utilized identical omnidirectional sleeve dipole antennas with $+2.3$ dBi gain (Mobile Mark model PSKN3-24/55S). Two individual scenarios were considered for the LOS and NLOS channel conditions where the test subject walked towards and then away from the RX in a straight line, from the 9 m point to 1 m point and vice versa. It is worth remarking that the NLOS conditions corresponded to the condition where the human body obscured the direct communication path between the wearable node and the RX.

To abstract the composite fading signal for the wearable off-body measurements, the estimated path loss was removed from the raw measurement data using the log-distance path loss given in [42, Eq. (3.68)]. To this end, the elapsed time was first converted into a distance based upon an estimate of the test subject's velocity. The corresponding parameter estimates for the η-μ / inverse gamma (*Format* 1) composite fading model were obtained using a non-linear least squares routine programmed in MATLAB to fit (2) to the wearable off-body measurement data [3]. The minimum data set size used for the parameter estimations was 2331 for the wearable off-body channel measurements. The goodness-of-fit of the considered composite model was evaluated using the RAD [43] which is a symmetric version of the Kullback-Leibler divergence (KLD) [44]. Unlike the KLD, the RAD satisfies the triangle inequality, which constitutes it a true distance metric. As an example of the model fitting, Fig. 2 shows the PDF of the η-μ / inverse gamma composite fading model fitted to the measurement data for the LOS and NLOS wearable off-body channels within the two different environments. It is clear that the η-μ / inverse gamma composite fading model provided a good fit to the empirical data for all of the considered cases.

D. Application in Cellular Communication Channels

The use of device-to-device (D2D) communications has recently been proposed to supplement traditional cellular communications by providing higher data rates and extending the coverage of cellular networks [3] and the reference therein. In this context, D2D communications will be achieved by using network users themselves as ad hoc base stations to facilitate the routing of data traffic and to relay broadcasts. For the D2D measurements conducted in this study, the TX and RX antennas were securely fixed to the inside of a compact acrylonitrile butadiene styrene (ABS) enclosure (107 mm $\times$ 55 mm $\times$ 20 mm) using a small strip of Velcro®. This configuration for the hypothetical User Equipment (UE)

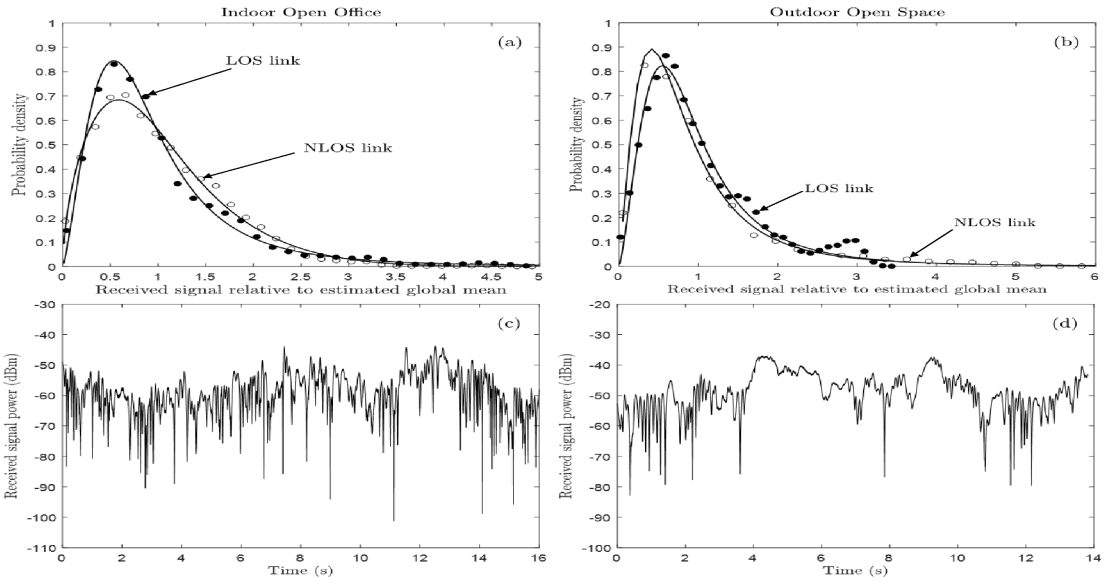

Fig. 3: Empirical (symbols) and theoretical PDFs for the η-μ / inverse gamma (dotted lines) models for the LOS and NLOS D2D links in the (a) indoor open office and (b) outdoor open space environments alongside the received signal power for the LOS link in the (c) indoor open office and (d) outdoor open space environments.

mimicked the form of a smart phone which allowed the user to emulate making a voice call as they would normally. Similar to the wearable off-body measurement set up, the wireless node used for the TX consisted of an ML5805 transceiver and was configured to transmit a continuous wave signal with an output power of $+17.6$ dBm at 5.8 GHz. The wireless node used for the RX also featured an ML5805 transceiver attached to a PIC32MX which acted as a baseband controller, allowing the analog received signal strength (RSS) output to be sampled with a 10-bit quantization depth at a rate of 10 kHz. The utilized TX and RX antennas were the same as those used for the wearable off-body measurements which were connected to the wireless nodes using low-loss coaxial cables.

The D2D measurements were performed at 5.8 GHz in two different environments, namely (a) an indoor open office area environment and (b) an outdoor open space environment. The open office area is the same environment where the wearable off-body measurements were conducted. During the D2D measurements, the open office area was unoccupied in order to facilitate pedestrian free D2D channel measurements. The outdoor D2D measurements were conducted in an open space close to the ECIT building. In this study, the D2D link was formed between two persons, namely person A, an adult male of height 1.83 m and weight 73 kg, and person B, a female of height 1.65 m and weight 51 kg. It should be noted that the UEs used by persons A and B are denoted as UE_1 and UE_2, respectively. For all of the D2D measurements, persons A and B held the respective UE at their left ear to imitate making a voice call. Both test subjects were initially stationary, after which they were instructed to walk around randomly within a circle of radius of 0.5 m from their starting points.

It is worth highlighting that for the LOS D2D measurements in both environments, while there may have been a direct LOS between the two person's bodies during the trials, in actual fact, the link between the hypothetical UEs would have been subject to quasi-LOS conditions due to the random movements undertaken. For the NLOS case, person B was always positioned around an adjacent corner to ensure that the NLOS conditions (i.e. no direct path between persons A and B) were maintained irrespective of the random movements. In the analysis of the D2D channels, the global mean signal power was removed from the D2D measurement data to abstract the composite fading signal for field measurement data. Again, all parameter estimates for the η-μ / inverse gamma model were obtained using a non-linear least squares routine programmed in MATLAB to fit (2) to the D2D measurement data. It should be noted that the minimum data set size used for the parameter estimations was 138148 for the D2D measurements. As an example of the model fitting process, Figs. 3(a) and (b) illustrate the PDF of the η-μ / inverse gamma composite fading model fitted to the measurement data for both the LOS and NLOS D2D channels in the indoor and outdoor environments, respectively. It can be seen that the η-μ / inverse gamma model provided an adequate fit to the measurement data for the LOS and particularly for the NLOS conditions. Likewise, the measured received signal power time series for the LOS cases in both the indoor and outdoor environments is presented in Figs. 3(c) and (d). From these plots, it is clear that the received signal experienced longer-term fading due to the shadowing caused by both users, strongly advocating the use of a composite fading model in these cases, which are encountered in practical communications scenarios [3].

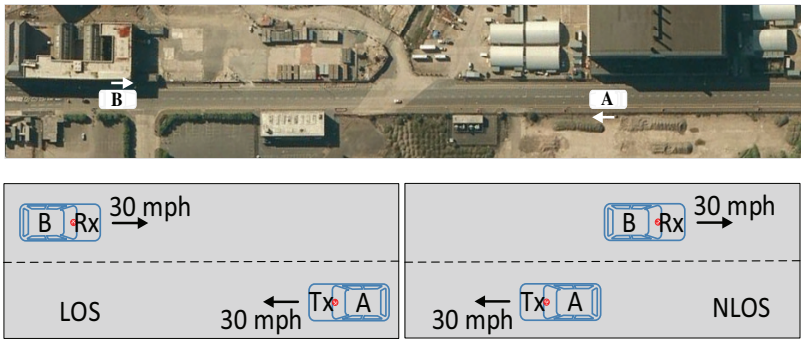

Fig. 4: Satellite view of V2V measurement environment showing the position of two vehicles and two different scenarios (LOS and NLOS channel conditions). It should be noted that the road is approximately 10 m in width.

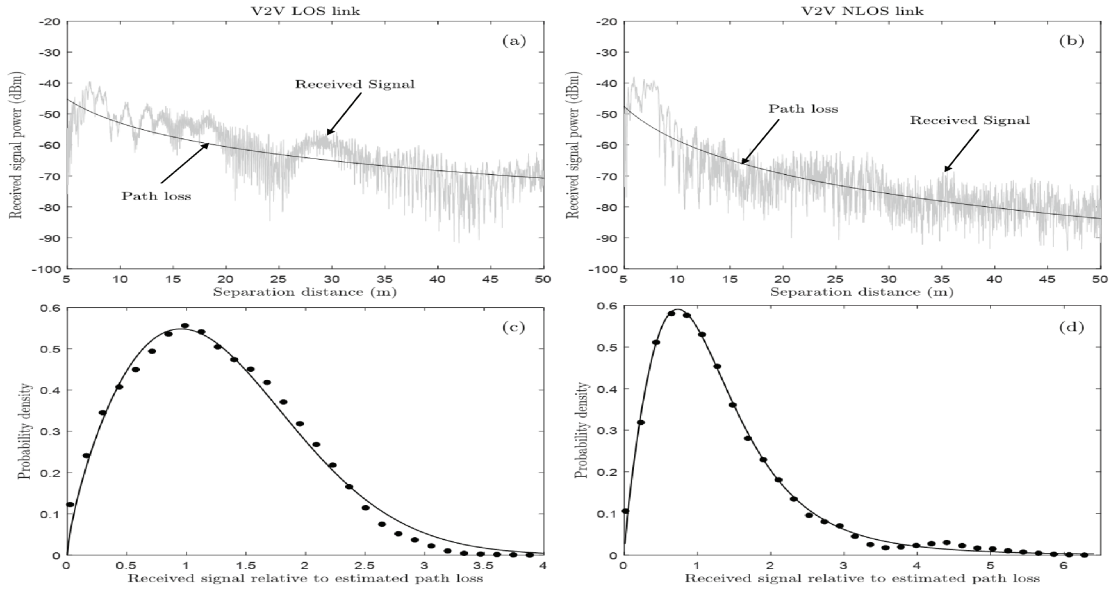

Fig. 5: Received signal power with a superimposed path loss fit for (a) the V2V LOS link and (b) the V2V NLOS link and empirical (circles) and theoretical PDF for the η-μ / inverse gamma (dotted lines) models for (c) the V2V LOS link and (d) the V2V NLOS link.

E. Application in Vehicular Communication Channels

Vehicular communications have become increasingly popular due to their potential for improving traffic safety and avoiding congestion [3] and the references therein. V2V channels exist between wireless devices situated on one vehicle and those situated on another vehicle. In the V2V channel measurements in [3], the utilized TX was the same as the previous cases since it was configured to generate a continuous wave signal with an output power of $+17.6$ dBm at 5.8 GHz. The RX was the identical wireless node used for the D2D measurements, but unlike the D2D measurements, the channel sampling frequency was 1 kHz. The V2V measurements were conducted in a business district environment in the Titanic Quarter of Belfast in the United Kingdom as shown in Fig. 4. For the V2V measurements, the TX was positioned on the center of the dash board of vehicle A, namely a Vauxhall (Opel in continental Europe) Zafira SRi using a small strip of Velcro® while the RX was mounted on the dash board of vehicle B, namely a Vauxhall Astra SRi. The measurement area consisted of a straight road with a number of office buildings nearby. To create the LOS and NLOS channel conditions, both vehicles A and B initially moved towards each other with a speed of 30 mph before passing and continuing their onward journey as shown in Fig. 4. A distance of 50 m on either side of the intersection point was considered for the LOS and NLOS analysis performed in this study [3]. Although the V2V channel measurements were performed during off-peak traffic hours, there still existed pedestrians and other vehicular traffic in the vicinity of vehicles A and B.

Similar to the wearable off-body analysis, the estimated path loss was removed from the V2V measurement data using the log-distance path loss to abstract the composite fading signal from the field measurement data. To this end, the elapsed time was first converted into a distance based

upon the vehicle's velocity. Also, the minimum data set size used for the parameter estimations was 13287 for the V2V measurements. As an example of the model fitting process, Fig. 5 shows the PDFs of the η-μ / inverse gamma composite fading model fitted to the LOS and NLOS V2V measurement data in conjunction with their respective received signal power time series. Also shown is the estimated path loss which was calculated using a reference distance of 5 m, which was the separation distance between the TX on vehicle A and the RX on vehicle B. It can be seen that the η-μ / inverse gamma composite fading model was in good agreement with the LOS and NLOS measurement data. As a result, it is evident that the proposed model constitutes an adequate solution for modeling versatile realistic scenarios such as those encountered in wearable, cellular and vehicular communications. In addition, its relatively convenient algebraic representation renders it tractable to handle both analytically and numerically. This is particularly advantageous in the analysis of complex systems, which is typically the case in emerging communications.

III. Ergodic Capacity over $\eta-\mu$ / Inverse Gamma Fading Channels

Ergodic capacity is a fundamental measure in wireless communications as it is largely associated with the quality of service requirements. It is well known that multipath fading and shadowing phenomena affect significantly the ergodic capacity. Based on this, this section is devoted to the ergodic capacity analysis of digital communications over the considered η-μ / inverse gamma composite fading channels. This analysis leads to some insights which will be useful in the design and deployment of future wireless systems in the context of wearable, cellular and vehicular communications, among others.

Theorem 1. *For $\mu, \overline{\gamma}, B \in \mathbb{R}^+$, $m_s \in \mathbb{N}$, $\eta \in \mathbb{R}^+$ in Format 1 and $-1 < \eta < 1$ in Format 2, the following analytic expression is valid for the ergodic capacity over η-μ / inverse gamma fading channels:*

$$\begin{aligned}\frac{C_e}{B} &= \frac{2^{1-2\mu}\sqrt{\pi}\Gamma(m_s+2\mu)}{h^{\mu}\Gamma(m_s)\Gamma(\mu)\Gamma\left(\mu+\frac{1}{2}\right)\ln(2)} \\ &\times \Bigg\{\sum_{i=0}^{\infty}\sum_{l=0}^{m_s-1}\binom{m_s-1}{l}(-1)^l H^{2i} \\ &\quad\times \frac{\left(\frac{m_s}{2}+\mu\right)_i\left(\frac{m_s+1}{2}+\mu\right)_i}{i!h^{2i}\left(\mu+\frac{1}{2}\right)_i}\Bigg[\frac{\ln(m_s\overline{\gamma})-\ln(2\mu h)}{2i+2\mu+l} \\ &\quad+\frac{B\left(1-\frac{m_s\overline{\gamma}}{2\mu h},1+2i+2\mu+l,0\right)}{(2i+2\mu+l)\left(1-\frac{m_s\overline{\gamma}}{2\mu h}\right)^{2i+2\mu+l}}\Bigg] \\ &\quad+\sum_{i=0}^{\infty}\sum_{l=0}^{m_s-1}\sum_{j=1}^{2i+2\mu+l}\binom{m_s-1}{l} \\ &\quad\times\frac{(-1)^l H^{2i}\left(\frac{m_s}{2}+\mu\right)_i\left(\frac{m_s+1}{2}+\mu\right)_i}{ji!h^{2i}(2\mu+2i+l)\left(\mu+\frac{1}{2}\right)_i}\Bigg\}.\end{aligned} \tag{11}$$

Proof. By substituting the SNR PDF of the η-μ / inverse gamma distribution in [3, Eq. (13)] into

$$C_e \triangleq B\int_0^{\infty}\log_2(1+\gamma)p_{\gamma}(\gamma)\mathrm{d}\gamma \tag{12}$$

and setting $u = 2\mu h\gamma + m_s\overline{\gamma}$, one obtains

$$\begin{aligned}\frac{C_e}{B} &= \frac{\sqrt{\pi}2^{1-2\mu}m_s^{m_s}\overline{\gamma}^{m_s}\Gamma(m_s+2\mu)}{h^{\mu}\Gamma(m_s)\Gamma(\mu)\Gamma\left(\mu+\frac{1}{2}\right)}\times \\ &\int_0^{\infty}\frac{(u-m_s\overline{\gamma})^{2\mu-1}}{u^{m_s+2\mu}}\log_2\left(1+\frac{u-m_s\overline{\gamma}}{2\mu h}\right) \\ &\quad{}_2F_1\left(\frac{m_s}{2}+\mu,\frac{m_s+1}{2}+\mu;\mu+\frac{1}{2};\left(\frac{H(u-m_s\overline{\gamma})}{hu}\right)^2\right)\mathrm{d}u.\end{aligned} \tag{13}$$

By also setting $t = 1 - m_s\overline{\gamma}/u$, and after some algebraic manipulations, it follows that

$$\begin{aligned}\frac{C_e}{B} =& \frac{2^{1-2\mu}\sqrt{\pi}\Gamma(m_s+2\mu)}{\Gamma(m_s)\Gamma(\mu)\Gamma\left(\mu+\frac{1}{2}\right)h^{\mu}}\times \\ &\Bigg\{\int_0^1\frac{t^{2\mu-1}}{(1-t)^{1-m_s}}\log_2\left(1-\left(1-\frac{m_s\overline{\gamma}}{2\mu h}\right)t\right) \\ &\quad\times{}_2F_1\left(\frac{m_s}{2}+\mu,\frac{m_s+1}{2}+\mu;\mu+\frac{1}{2};\frac{H^2t^2}{h^2}\right)\mathrm{d}t \\ &+\int_0^1\frac{t^{2\mu-1}\log_2(1-t)}{(1-t)^{1-m_s}} \\ &\quad\times{}_2F_1\left(\frac{m_s}{2}+\mu,\frac{m_s+1}{2}+\mu;\mu+\frac{1}{2};\frac{H^2t^2}{h^2}\right)\mathrm{d}t\Bigg\}.\end{aligned} \tag{14}$$

To this effect and with the aid of [38, Eq. (1.111)] and expanding out the involved logarithmic terms and the hypergeometric function using [38, Eq. (9.14.1)], it follows that

$$\begin{aligned}\frac{C_e}{B} &= \frac{2^{1-2\mu}\sqrt{\pi}\Gamma(m_s+2\mu)}{\Gamma(m_s)\Gamma(\mu)\Gamma\left(\mu+\frac{1}{2}\right)h^{\mu}} \\ &\quad\times\sum_{l=0}^{m_s-1}\sum_{i=0}^{\infty}\binom{m_s-1}{l}\frac{(-1)^l\left(\frac{m_s}{2}+\mu\right)_i\left(\frac{m_s+1}{2}+\mu\right)_i}{i!h^{2i}H^{-2i}\left(\mu+\frac{1}{2}\right)_i} \\ &\quad\times\Bigg\{\int_0^1 t^{2\mu+2i+l-1}\log_2\left(1-\left(1-\frac{m_s\overline{\gamma}}{2\mu h}\right)t\right) \\ &\quad-\int_0^1 t^{2\mu+2i+l-1}\log_2(1-t)\,\mathrm{d}t\Bigg\}.\end{aligned} \tag{15}$$

Notably, the above integrals can be expressed in closed-form with the aid of [38, Eq. (2.729.1)]. Therefore, by performing the necessary variable transformation and substituting in (15), equation (11) is deduced, which completes the proof. □

It is evident that the derived ergodic capacity expression is given in terms of an infinite series. This series is fully convergent and it can be sufficiently truncated after relatively few terms. However, determining the exact accuracy achieved for an arbitrary number of terms is essential. Based on this, we derive an upper bound for the involved truncation error of (11). This is tight and has a rather tractable algebraic

representation that renders it convenient to handle analytically and numerically.

Proposition 1. *For $\mu, \overline{\gamma}, B \in \mathbb{R}^+$, $m_s \in \mathbb{N}$, $\eta \in \mathbb{R}^+$ in Format 1 and $-1 < \eta < 1$ in Format 2, the following closed-form upper bound holds for the truncation error of* (11)

$$\begin{aligned}\mathcal{T} < & \sum_{l=0}^{m_s-1} \binom{m_s-1}{l} (-1)^l \\ & \times {}_2F_1\left(\frac{m_s}{2}+\mu, \frac{m_s+1}{2}+\mu; \mu+\frac{1}{2}; \frac{H^2}{h^2}\right) \\ & \times \left\{ \frac{\log(\overline{\gamma} m_s) - \log(2\mu h)}{2p+l+2\mu} + \sum_{j=1}^{2p+2\mu+l} \frac{1}{j!(2p+2\mu+l)} \right. \\ & \left. + \frac{B(1-\frac{\overline{\gamma} m_s}{2\mu h}, 1+2p+l+2\mu)}{(2p+2\mu+l)\left(1-\frac{\overline{\gamma} m_s}{2\mu h}\right)^{2p+2\mu+l}} \right\}\end{aligned} \tag{16}$$

where p denotes the number of terms of the series.

Proof. It is readily noticed that (11) can be upper bounded according to (17), at the top of the next page. Based on this and after some algebraic manipulations, it follows that the truncation error for the involved infinite series can be upper bounded as

$$\begin{aligned}\mathcal{T} < & \frac{2^{1-2\mu}\sqrt{\pi}\Gamma(m_s+2\mu)}{h^\mu \Gamma(m_s)\Gamma(\mu)\Gamma\left(\mu+\frac{1}{2}\right)\log(2)} \\ & \times \left\{ \sum_{i=p}^{\infty} \sum_{l=0}^{m_s-1} \binom{m_s-1}{l} \frac{(-1)^l \left(\mu+\frac{m_s}{2}\right)_i \left(\mu+\frac{m_s+1}{2}\right)_i}{i! h^{2i} H^{-2i} \left(\mu+\frac{1}{2}\right)_i} \right. \\ & \times \left[\frac{\log(m_s\overline{\gamma}) - \log(2\mu h)}{2p+2\mu+l} \right. \\ & \left. + \frac{B\left(1-\frac{m_s\overline{\gamma}}{2\mu h}, 1+2p+2\mu+l\right)}{(2p+2\mu+l)\left(1-\frac{m_s\overline{\gamma}}{2\mu h}\right)^{2p+2\mu+l}} \right] \\ & + \sum_{i=p}^{\infty} \frac{H^{2i}\left(\frac{m_s}{2}+\mu\right)_i \left(\frac{m_s+1}{2}+\mu\right)_i}{i! h^{2i} \left(\frac{1}{2}+\mu\right)_i} \\ & \left. \times \sum_{l=0}^{m_s-1} \binom{m_s-1}{l} \frac{(-1)^l}{2p+2\mu+l} \sum_{j=1}^{2p+2\mu+l} \frac{1}{j!} \right\}.\end{aligned} \tag{18}$$

By setting $p = 0$ and recalling the properties of Pochhammer symbol and hypergeometric functions, it is noticed that the resulting infinite series can be expressed in closed-form in terms of the generalized hypergeometric function. To this effect and after some algebraic manipulations, equation (16) is deduced, which completes the proof. □

It is evident that the derived analytic expressions have a tractable algebraic representation that allows their straightforward computation, since the involved functions are included as built-in functions in popular software packages such as MATLAB, MAPLE and MATHEMATICA.

IV. Numerical Results

This section employs the derived results from the previous sections in the quantification of the effects of composite multipath/shadowing conditions on the ergodic capacity, as this can occur in realistic communications scenarios undergoing fading effects, such as in wearable, cellular and vehicular communication scenarios. To this end, Fig. 6 illustrates the ergodic capacity over $\eta-\mu$ / inverse gamma composite fading channels. It is evident that the joint effects of multipath fading and shadowing are considerable as significant deviations from the often assumed case of Rayleigh fading are observed. For example, a change of around 20% spectral efficiency is observed when μ changes from $\mu = 0.3$ to $\mu = 1.0$, for the case of $\eta = 5.0$, $m_s = 9.0$ and moderate average SNR values, such as $\overline{\gamma} = 10$dB. It is also noticed that the same variation is largely observed at low and particularly at moderate and high SNR regimes, which verifies the crucial effect of multipath clusters on the overall system performance. In the same context, a spectral efficiency deviation of approximately 15% is observed for different shadowing severity across the whole average SNR range and for fixed values of μ and η parameters. Likewise, a variation of around 10% is observed at low, moderate and high average SNR values when η is changed while μ and m_s remain fixed.

As a result, it is evident that each individual fading parameter of the $\eta-\mu$ / inverse gamma composite fading model has a critical effect on the overall capacity levels. Also, when more than one of the parameters change simultaneously, which is expected in realistic mobile communication scenarios, the corresponding ergodic capacity changes are considerably greater, since variations of around 50% are shown for certain fading scenarios across the whole SNR range. Also, it is evident that the modeling versatility of the proposed model is significantly more realistic than the simplistic Rayleigh fading case since large variations are observed between the two models across the whole SNR range. This typically corresponds to gains of several dBs for fixed spectral efficiencies, which is particularly advantageous in emerging applications which demand substantially increased quality of service and low-power requirements. In fact, this also concerns wireless power transfer based applications as these extra power levels can, for example, assist in the powering of low power devices. Therefore, it is evident that the offered results verify that accurate characterization and modeling of multipath fading and shadowing effects are of paramount importance in the design of emerging communication technologies, such as wearable and vehicular communication systems, among others.

V. Conclusion

This work was devoted to the ergodic capacity analysis of digital communications over $\eta-\mu$ / inverse gamma fading channels. First, the main theoretical and practical characteristics of the recently proposed $\eta-\mu$ / inverse gamma fading model were revisited along with a detailed description of its modeling capability in the context of wearable, cellular and vehicular communications. Capitalizing on this, novel

$$C_e < \frac{2^{1-2\mu}\sqrt{\pi}\Gamma(m_s+2\mu)}{h^{\mu}\Gamma(m_s)\Gamma(\mu)\Gamma\left(\mu+\frac{1}{2}\right)\log(2)} \left\{ \sum_{i=0}^{\infty}\sum_{l=0}^{m_s-1} \binom{m_s-1}{l} \frac{(-1)^l H^{2i}\left(\frac{m_s}{2}+\mu\right)_i \left(\frac{m_s+1}{2}+\mu\right)_i}{i!h^{2\mu}\left(\mu+\frac{1}{2}\right)_i} \right.$$
$$\times \frac{1}{2\mu+2i+l}\left[\log\left(\frac{m_s\overline{\gamma}}{2\mu h}\right) + B\left(1-\frac{m_s\overline{\gamma}}{2\mu h}, 1+2i+l+2\mu, 0\right)\left(1-\frac{m_s\overline{\gamma}}{2\mu h}\right)^{-2i-2\mu-l}\right] \tag{17}$$
$$\left. + \sum_{i=0}^{\infty}\sum_{l=0}^{m_s-1}\sum_{j=1}^{2i+2\mu+l} \binom{m_s-1}{l} \frac{(-1)^l H^{2i}\left(\mu+\frac{m_s}{2}\right)_i \left(\mu+\frac{m_s+1}{2}\right)_i}{i!j!h^{2i}(2i+2\mu+l)\left(\mu+\frac{1}{2}\right)_i} \right\}.$$

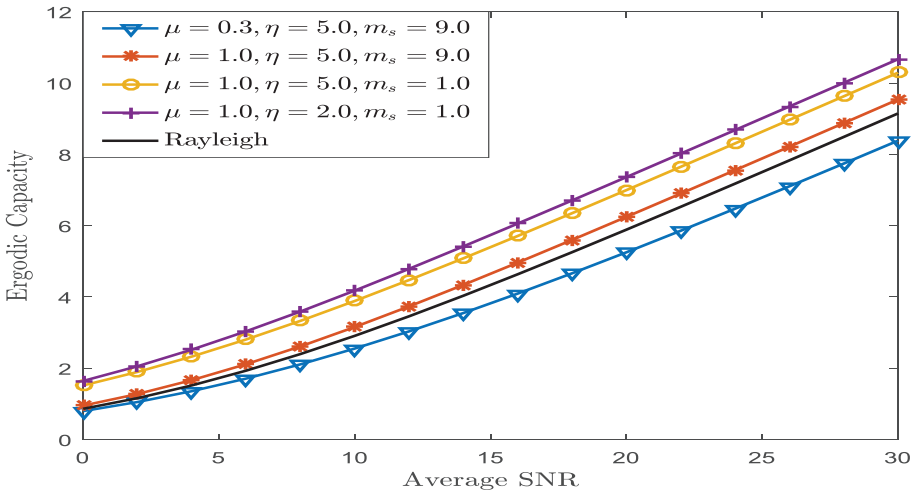

Fig. 6: Ergodic capacity versus average SNR under $\eta-\mu$ / inverse gamma fading channels for different μ, η and m_s values.

exact analytic expressions were derived for the corresponding ergodic capacity which were subsequently employed in quantifying the effects of severity of multipath fading and shadowing fading conditions on the performance of the considered set ups. It was shown that the effect of different types of composite fading have a considerable effect across all SNR regimes. These effects are clearly beyond the range of the conventional Rayleigh distributed multipath fading effects and thus, they must be taken into account in the realistic design and deployment of emerging wireless systems. This is of paramount importance since future systems will be largely characterized by significantly increased quality of service and low power requirements. Indicative examples include timely and critical topics of interest such as wearable, cellular and vehicular communications. In addition, realistic channel modeling can be useful in the context of wireless power transfer, which is a core topic of the Internet of Things (IoT) paradigm. This is because various target quality of service requirements can be met at a reduced power levels in non-severe fading conditions, which insinuates that any remaining power can be dedicated to the wireless powering of low power communication devices.

ACKNOWLEDGMENTS

This work was supported in part by the U.K. Engineering and Physical Sciences Research Council under Grant No. EP/L026074/1, by the Department for the Economy Northern Ireland through Grant No. USI080 and by the Academy of Finland under projects 284694 and 288670.

REFERENCES

[1] S. Ki Yoo, S. L. Cotton, P. C. Sofotasios, M. Matthaiou, M. Valkama, G. K. Karagiannidis, "The $\kappa-\mu$ / inverse gamma fading model," *in IEEE PIMRC '15*, Hong Kong, Aug/Sep. 2015, pp. 949−953.

[2] S. Ki Yoo, P. C. Sofotasios, S. L. Cotton, M. Matthaiou, M. Valkama, G. K. Karagiannidis, "The $\eta-\mu$/ inverse gamma composite fading model," *in IEEE PIMRC '15*, Hong Kong, Aug/Sep. 2015, pp. 978−982.

[3] S. K. Yoo, N. Bhargav, S. L. Cotton, P. C. Sofotasios, M. Matthaiou, M. Valkama, and G. K. Karagiannidis, "The κ-μ / inverse gamma and η-μ / inverse gamma composite fading models: Fundamental statistics and empirical validation," *IEEE Trans. Commun.*, To Appear.

[4] J. F. Paris, "Advances in the statistical characterization of fading: From 2005 to present," *HINDAWI Int. J. Antennas and Propag.*, vol. 2014, Article ID 258308.

[5] S. Ki Yoo, S. L. Cotton, P. C. Sofotasios, and S. Freear, "Shadowed fading in indoor off-body communications channels: A statistical characterization using the $\kappa-\mu$/gamma composite fading model," *IEEE Trans. Wireless Commun.*, vol. 15, no. 8, pp. 5231−5244, Aug. 2016.

[6] M. K. Simon, and M.-S. Alouini, *Digital Communication over Fading Channels*, 2nd edn., Wiley, New York, 2005.

[7] M. D. Yacoub, "The $\alpha-\mu$ distribution: A physical fading model for the Stacy distribution," *IEEE Trans. Veh. Technol.*, vol. 56, no. 1, pp. 27−34, Jan. 2007.

[8] M. D. Yacoub, "The $\kappa-\mu$ distribution and the $\eta-\mu$ distribution," *IEEE Antennas Propag. Mag.*, vol. 49, no. 1, pp. 68−81, Feb. 2007.

[9] F. J. Lopez-Martinez, E. Martos-Naya, D. Morales-Jimenez, and J. F. Paris, "On the bivariate Nakagami$-m$ cumulative distribution function: closed-form expressions and applications," *IEEE Trans. Commun.*, vol. 61, no. 4, pp. 1404−1414, Apr. 2013.

[10] M. A. G. Villavicencio, R. A. A. de Souza, G. C. de Souza, and M. D. Yacoub, "A bivariate $\kappa - \mu$ distribution," *IEEE Trans. Veh. Technol.*, vol. 65, no. 7, pp. 5737−5743, July 2016.

[11] A. Abdi, and M. Kaveh, "$K-$distribution: An appropriate substitute for Rayleigh-lognormal distribution in fading-shadowing wireless channels," *IET Electron. Lett.*, vol. 34, no. 9, pp. 851−852, Apr. 1998.

[12] P. S. Bithas, "Weibull-gamma composite distribution: Alternative multipath/shadowing fading model," *IET Electron. Lett.*, vol. 45, no. 14, July 2009.

[13] A. Laourine, M.-S. Alouini, S. Affes, and A. Stephenne, "On the performance analysis of composite multipath/shadowing channels using the $G-$distribution," *IEEE Trans. Commun.*, vol. 57, no. 4, pp. 1162−1170, Apr. 2009.

[14] N. D. Chatzidiamantis, and G. K. Karagiannidis, "On the distribution of the sum of gamma-gamma variates and applications in RF and optical wireless communications," *IEEE Trans. Commun.*, vol. 59, no. 5, pp. 1298−1308, May 2011.

[15] J. F. Paris, "Statistical characterization of κ-μ shadowed fading," *IEEE Trans. Veh. Technol.*, vol. 63, no. 2, pp. 518−526, Feb. 2014.

[16] S. L. Cotton, "Human body shadowing in cellular device-to-device communications: Channel modeling using the shadowed κ-μ fading model," *IEEE J. Sel. Areas Commun.*, vol. 33, no. 1, pp. 111−119, Jan. 2015.

[17] L. Moreno-Pozas, F. J. Lopez-Martinez, J. F. Paris, and E. Martos-Naya, "The $\kappa - \mu$ shadowed fading model: Unifying the κ-μ and η-μ distributions, *IEEE Trans. Veh. Technol.*, vol. 65, no. 12, pp. 9630−9641, Dec. 2016.

[18] F. J. Lopez-Martinez, J. F. Paris, and J. M. Romero-Jerez, "The $\kappa - \mu$ shadowed fading model with integer fading parameters," *IEEE Trans. Veh. Technol.*, vol. 66, no. 9, pp. 7653−7662, Sep. 2017.

[19] S. K. Yoo, S. L. Cotton, P. C. Sofotasios, M. Matthaiou, M. Valkama, and G. K. Karagiannidis, "The Fisher−Snedecor F distribution: A simple and accurate composite fading model," *IEEE Commun. Lett.*, vol. 21, no. 7, pp. 1661−1664, Jul. 2017.

[20] P. C. Sofotasios, *On Special Functions and Composite Statistical Distributions and Their Applications in Digital Communications over Fading Channels*, Ph.D. Dissertation, University of Leeds, England, UK, 2010.

[21] P. C. Sofotasios, T. A. Tsiftsis, M. Ghogho, L. R. Wilhelmsson, and M. Valkama, "The $\eta - \mu$/inverse-Gaussian distribution: A novel physical multipath/shadowing fading model," *in 2013 IEEE ICC '13*, Budapest, Hungary, Jun. 2013, pp. 5715−5719.

[22] S. Harput, P. C. Sofotasios, and S. Freear, "A novel composite statistical model for ultrasound applications," *in IEEE International Ultrasonics Symposium (IUS '11)*, Orlando, FL, USA, Oct. 2011, pp. 1−4.

[23] P. C. Sofotasios, T. A. Tsiftsis, K. Ho-Van, S. Freear, L. R. Wilhelmsson, and M. Valkama, "The $\kappa - \mu$/inverse-Gaussian composite statistical distribution in RF and FSO wireless channels," *in IEEE VTC 13 - Fall*, Las Vegas, NV, USA, Sep. 2013, pp. 1−5.

[24] A. J. Goldsmith, and P. P. Varaiya, "Capacity of fading channels with channel side information," *IEEE Trans. Inf. Theory*, vol. 43, no. 6, pp. 1986−1992, Nov. 1997.

[25] I. M. Kostic, "Analytical approach to performance analysis for channel subject to shadowing and fading," *IEE Proc. Commun.*, vol. 152, no. 6, pp. 821−827, Dec. 2005.

[26] D. Benevides da Costa, and M. D. Yacoub, "Average channel capacity for generalized fading scenarios," *IEEE Commun. Lett.*, vol. 11, no. 12, pp. 949−951, Dec. 2007.

[27] P. S. Bithas, G. P. Efthymoglou, and N. C. Sagias, "Spectral efficiency of adaptive transmission and selection diversity on generalized fading channels," *IET Commun.*, vol. 4, no. 17, pp. 2058−2064, 2010.

[28] N. Y. Ermolova, and O. Tirkkonen, "The $\eta - \mu$ fading distribution with integer values of μ," *IEEE Trans. Wireless Commun.*, vol. 10, no. 6, pp. 1976−1982, Jun. 2011.

[29] P. S. Bithas, N. C. Sagias, P. T. Mathiopoulos, and G. K. Karagiannidis, "On the performance analysis of digital communications over generalized fading channels," *IEEE Commun. Lett.*, vol. 10, no. 5, pp. 353−355, May 2006.

[30] C. Zhong, M. Matthaiou, G. K. Karagiannidis, and T. Ratnarajah, "Generic ergodic capacity bounds for fixed-gain AF dual-hop relaying systems," *IEEE Trans. Wireless Commun.*, vol. 60, no. 8, pp. 3814−3824, Oct. 2011.

[31] J. Zhang, M. Matthaiou, Z. Tan, and H. Wang, "Performance analysis of digital communication systems over composite η-μ / gamma fading channels," *IEEE Trans. Veh. Technol.*, vol. 61, no. 7, pp. 3114−3124, Sep. 2012.

[32] C. Garca-Corrales, F. J. Canete, and J. F. Paris, "Capacity of κ-μ shadowed fading channels," *HINDAWI Int. J. Antennas and Propag.*, pp. 1−8, July 2014.

[33] J. F. Paris, "Outage probability in η-μ / η-μ and κ-μ / η-μ interference-limited scenarios," *IEEE Trans. Commun.*, vol. 61, no. 1, pp. 335−343, Jan. 2013.

[34] G. George, R. K. Mungara, and A. Lozano, "An analytical framework for device-to-device communication in cellular networks," *IEEE Trans. Wireless Commun.*, vol. 14, no. 11, pp. 6297−6310, Jul. 2015.

[35] L. Wei, Z. Zheng, J. Corander, and G. Taricco, "On the outage capacity of orthogonal space-time block codes over multi-cluster scattering MIMO channels," *IEEE Trans. Commun.*, vol. 63, no. 5, pp. 1700−1711, May 2015.

[36] C. Kourogiorgas, S. Sagkriotis, and A. D. Panagopoulos, "Coverage and outage capacity evaluation in 5G millimeter wave cellular systems: impact of rain attenuation," 9^{th} *EuCAP '15*, Apr. 2015, Lisbon, Portugal, pp. 1−5.

[37] F. Hansen and F. I. Meno, "Mobile fading - Rayleigh and lognormal superimposed," *IEEE Trans. Veh. Technol.*, vol. 26, no. 4, pp. 332–335, Nov. 1977.

[38] I. S. Gradshteyn, and I. M. Ryzhik, *Tables of Integrals, Series, and Products*, in 7^{th} ed. Academic, New York, 2007.

[39] V. M. Kapinas, S. K. Mihos, and G. K. Karagiannidis, "On the Monotonicity of the Generalized Marcum and Nuttall Q-Functions," *IEEE Trans. Inf. Theory*, vol. 55, no. 8, pp. 3701−3710, Aug. 2009.

[40] A. P. Prudnikov, Yu. A. Brychkov, and O. I. Marichev, *Integrals and Series*, Gordon and Breach Science, vol. 3, More Special Functions, 1992.

[41] A. P. Prudnikov, Yu. A. Brychkov, and O. I. Marichev, *Integrals and Series*, Gordon and Breach Science, vol. 2, Special Functions, 1992.

[42] T. S. Rappaport, *Wireless communications: Principles and practice*. New Jersey: Prentice Hall PTR, 2002.

[43] D. H. Johnson and S. Sinanovic, *Symmetrizing the Kullback-Leibler distance*. Rice University Working Paper, 2001.

[44] S. Kullback, *Information theory and statistics*. Courier Corporation, 1997.